Published in "Journal of the European Ceramic Society 38(15): 5228–5233, 2018"
which should be cited to refer to this work.

Non-invasive Raman identification of crystalline and glassy phases in a 1781 Sèvres Royal Factory soft paste porcelain plate

Philippe Colomban[a,*], Marino Maggetti[b], Antoine d'Albis[c]

[a] Sorbonne Université, CNRS, MONARIS umr8233, Campus Pierre et Marie Curie, 4 Place Jussieu, 75005, Paris, France
[b] Department of Geosciences, Earth Sciences, University of Fribourg, Ch. du Musée 6, 1700 Fribourg, Switzerland
[c] 34, rue Saint-Lazare, 87000, Limoges, France

ARTICLE INFO

Keywords:
Fritware
Porcelain
Enamel
Blue
As-Pb apatite

ABSTRACT

A Raman study of a Sèvres soft paste (frit) porcelain plate allowed the identification of both the crystalline and amorphous phases. Cristobalite and pseudowollastonite gave main Raman signatures in the body where also tridymite, amorphous alkali silicate glass and lead arsenate apatite were detected. $Na_{0.4}K_{0.1}Ca_{0.5}Pb_4(AsO_4)_3$ lacunar apatite is identified as opacifier in blue and green overglaze enamel. Pb-Sb-reach pyrochlore (Naples Yellow) pigment was found in yellow and green overglaze enamels. The orange hue is obtained by superposing a hematite bearing red paint stroke over the yellow. These results are compared to those previously obtained by detailed OM, SEM, XRD and XRF analyses. Some of the phases identified by XRD (quartz, tridymite) are hardly detected by Raman and vice versa cristobalite was not found by XRD, most probably due to its low amount.

1. Introduction

Porcelain (also called 'china') made from kaolin, feldspar, and quartz is a Chinese innovation, a notable example of the great advancement in ceramic technique that occurred in China many centuries before reaching Europe [1]. One of the peculiar assets of porcelain is its whiteness, which allows the application of mono- and polychrome decorations. In the lack of kaolin, European potters developed an alternative procedure: the body doesn't result from the high temperature transformation of kaolin, feldspar and sand into a network of acicular mullite crystals in a glassy phase, but consists of white sand cemented with a glass, the frit [2]. The refractoriness of the latter being low, lead-based glaze was applied and fired at lower temperature ("Muffle" firing) than the potash-lime-based glaze covering china.

Getting a good 'coloured' decor requires a sufficient amount of chromophore but often its dispersion with a 'white' phase, the opacifier, in order to obtain a vivid and nice colour. This is the case for the blue overglaze enamel decor of porcelain achieved with cobalt. A too high concentration of chromophore darkens or even makes matte the colour. There are many ways to whiten a glass. All are based on the contrast between the refractive index of the dispersed phase with respect to that of the glassy matrix, the most simple way being the dispersion of bubbles with a size close to the human eyes resolution (1–10 μm) [3,4] or, as best alternative technique, the dispersion of phases with a high index of refraction, namely cassiterite (SnO_2) or lead arsenates [5–7]. Cassiterite is a stoichiometric phase and its identification is unambiguous, and this with many techniques. The possibility to form complex phases makes the identification of arsenate more difficult. Furthermore the literature on harmful to health compounds is limited. The availability of enamelled soft paste (frit) porcelain shards, decorated by Jean-Jacques Pierre le Jeune at Sèvres Royal Factory in 1781, which were previously comprehensively studied by a combination of techniques such as optical (OM) and scanning electron microscopy (SEM), X-ray diffraction (XRD) and X-ray fluorescence (XRF) [8], see Table 1, offers the possibility to compare the efficiency of the Raman microspectrometry for the identification of phases in this peculiar porcelain type. A previous study [9] has demonstrated that Raman spectroscopy mapping can be more efficient than X-ray diffraction to detect minor phases of pottery made of coarse grains as a spectrum can be measured for each grain. On the other hand, the smaller size of grains in porcelain body and glaze/enamel questions the efficiency of the Raman technique. We compare here the information obtained by non-invasive Raman scattering on enamelled soft paste porcelain shards and we try to characterize all the phases previously found by XRD and SEM, including amorphous ones. Results are discussed in the light of previous studies of different enamelled objects produced in ancient times.

The analysed colours belong, according to [8,10] to two groups: (1) Primary and (2) Secondary. The first encompasses the blue (labelled #1 in Fig. 1), yellow (#2), green (#3), purple (#7) and red. The second the

* Corresponding author.
E-mail address: philippe.colomban@sorbonne-universite.fr (P. Colomban).

Table 1
Summary of the results obtained with different methods (Optical microscopy OM, scanning electron microscopy SEM, X-ray diffraction XRD, X-ray fluorescence XRF) on the body, the glaze and the enamel colours [8].

Type	XRD	XRF	OM & SEM-BSE	SEM-EDS
Body	Wollastonite + tridymite +/- quartz	SiO_2- and CaO-rich	Wollastonite-rich patches with tridymite/quartz-rich domains & interstitial glass	Glass: SiO_2 and K_2O-rich. Wollastonite-rich patches: SiO_2-&CaO-rich
Glaze			Transparent homogeneous outer glass with a thick reaction zone (crystals & glass)	Outer glass: SiO_2-PbO-K_2O-CaO. Reaction zone: SiO_2-PbO-CaO-K_2O
Blue			Crystals (globules & dendrites) in a blue, glassy matrix	Crystals: Pb arsenates. Glassy matrix: Co-rich, PbO-SiO_2
Yellow			Pseudo-hexagonal crystals in a transparent glassy matrix	Crystals: Pb-Sb-Sn. Glassy matrix: SiO_2-PbO-rich
Green			Pseudo-hexagonal crystals in a blue-green glassy matrix	Crystals: Pb-Sb-Sn. Glassy matrix: Co- & Cu-bearing, SiO_2-PbO-rich
Red			Mix of yellow (pseudo-hexagonal crystals in a transparent glassy matrix) and red (homogeneous glass)	Yellow: Pb-Sb-crystals. Red: Fe-rich PbO-SiO_2-glass
Purple			Homogeneous purple glass with few SiO_2-crystals (cristobalite or tridymite) and drops of pure Au	Glass: PbO-SiO_2
Violet			Mix of blue and purple	

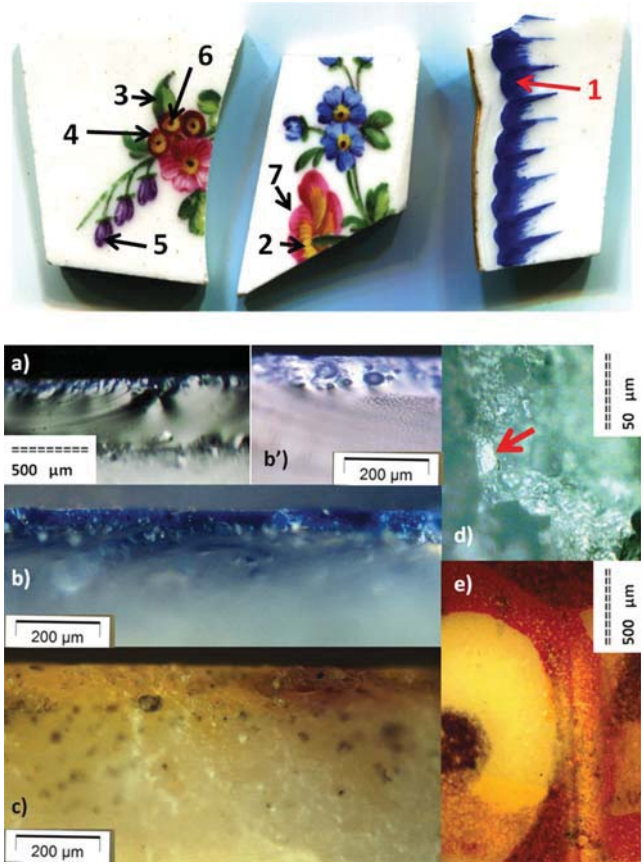

Fig. 1. Samples (above) showing blue(#1), yellow(#2), green(#3), orange (#4), violet(#5), black(#6) and purple(#7) enamels. Fracture sections: (a), (b) and (b') blue enamel; the blue enamel is laid on the glaze and crystals are present at the glaze-body interface; (c) yellow and orange; (d) body section showing a 'quartz' grain (red arrow) exhibiting a cristobalite Raman signature; (e) flower view from the top with yellow, red and orange enamels. (For interpretation of the references to color in this figure legend, the reader is referred to the web version of this article.)

violet (mauve)(#5), which the painter created by a mechanical mixture of blue and purple, as well as all the hues created by superimposing differently coloured brushstrokes, such as orange (red over yellow #4, see Fig. 1e) and "black" (see further) to brown (violet over green #6).

2. Samples and methods

Fig. 1 shows the three samples cut from a broken soft paste (frit) porcelain plate (private collection). According to the mark the plate was made at the Sèvres Royal Factory in 1781. More historical details can be found in previous papers [8,10]. Raman examination was also made on the fracture (section) and from the top, i.e. at the surface of the glaze and the enamels. A high sensitivity LABRAM Infinity Dilor spectrometer equipped with a 532 nm JDS-Uniphase YAG and a HORIBA Jobin-Yvon Peltier cooled CCD is first used to get a global view of the different Raman signatures. Illumination power varies from 5 to 0.5 mW at the sample. Backscattering measurements were made with Olympus standard and Long Working Distance x100 objectives. Twenty to thirty different spots were analysed for each shard in order to get a global survey (typical recording time: 2 to 10 min/spectrum). Complementary measurements were made with a HR800 HORIBA Jobin-Yvon spectrometer equipped with a similar CCD detector, but using a blue laser line (488 nm, Coherent Innova 90C Ar^+ ion laser) and variable microscope objectives (x10, x50 and X100 Olympus LMPlan).

3. Results and discussion

Figs. 2(left) and 3 show representative spectra recorded under green laser excitation on the body, the colourless glaze and on blue, yellow, green, orange and 'black' enamels; Figs. 4 to 6 spectra were recorded under blue laser excitation. Identified phases are listed in Table 2.

3.1. Body

Four crystalline phases and an amorphous one were found in the body in agreement with previous XRD and SEM investigations [8]. Pseudowollastonite (β-$CaSiO_3$), the marker of soft-paste (frit) porcelain, is identified by Raman scattering with its characteristic ca. 640-975 cm^{-1} strong doublet and smaller peaks at ca. 1050 and 410 cm^{-1} (Fig. 2b), in almost all spectra recorded with x50 objective and in many of those recorded with x100 one, as previously observed for soft-paste (frit) porcelain bodies [11–13]. A small wavenumber upshift is assigned to a matrix compression effect (stress). An intense α−cristobalite (SiO_2)doublet at ca. 230 and 415 cm^{-1} and a strong 780 cm^{-1} peak (Fig. 2a) [14,15], are observed in many spots with x100 objective, as commonly observed in bodies of this porcelain type [11,12]. At first examination, it is difficult to say if β-cristobalite is also present because the broader bands of the later phase (ca. 315, 780 and 880 cm^{-1} according [14]), makes their detection less obvious. If this phase is present, its amount will be less than the one of the α-phase. The observation of a broad peak at 830 cm^{-1} with x10 objective (Fig. 2, right)

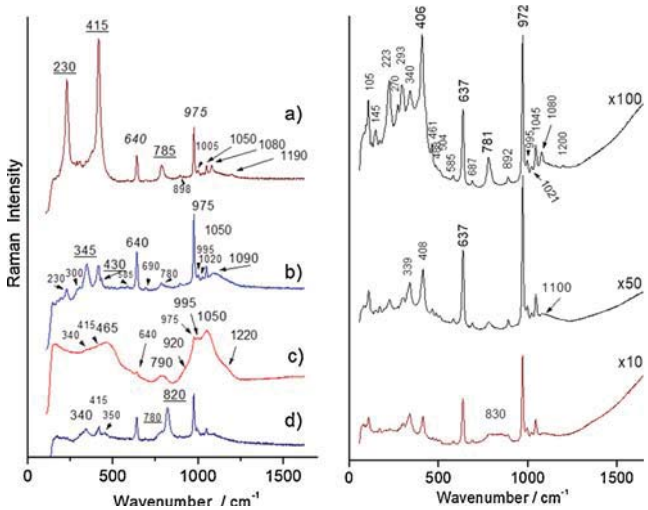

Fig. 2. Body: Left, representative spectra recorded under green laser excitation with x100 microscope objective; underlined wavenumbers are main peaks of α-cristobalite (a), α − tridymite (b) and lead arsenate apatite (d); (c) spectrum of the glassy intergranular phase; main peaks of each phase are underlined. Right, Raman spectra recorded under blue laser excitation on the body with x10, x50 and x100 objectives. (For interpretation of the references to color in this figure legend, the reader is referred to the web version of this article.)

can be consistent with the presence of β-cristobalite. Tridymite, another SiO_2 polymorph, clearly observed by XRD [8], was searched and only found in the α-tridymite form in regions where the optical image shows rather well defined grains. Its most characteristic peak is at ca. 345 cm^{-1} and for instance in rare spectra (Fig. 2,right, x100 objective) a broad and strong peak is observed at ~345 cm^{-1} [16,17]. Raman differentiation between the polymorphic modifications of tridymite is however poor documented, mixtures of tridymite and cristobalite are common [18] and the low intensity of the signal prevents better conclusions. We failed to detect α-quartz (this phase gives usually a very strong peak at ~465 cm^{-1} [11–13]) except as a very tiny component at 461 cm^{-1} for the x100 spectrum (Fig. 2), although this phase was unequivocally identified by XRD [8]. This puzzling fact could be due to the usual partial transformation of quartz grain's periphery into cristobalite [19] with a masking of the α-quartz Raman signature by the huge Raman intensity of the cristobalite spectrum. We recall that Raman intensity highly depends on the polarisability of the chemical bond, a highly variable parameter [20–22]. The spectrum of covalent bonded phase, especially those of high Z number (more electrons involved in the chemical bond, higher the corresponding Raman peaks), may mask the contribution of phase(s) made of more ionic bonds. This may explain the difficulty to observe clear tridymite signature (well detected by XRD) and the easiness to detect cristobalite (not observed by XRD) [8]. On the other hand, detection of a phase by XRD is known to succeed only if the content of this phase in a mixture is more than 5%, if it has a good cristallinity and is sufficiently large. As shown by the SEM-BSE images, cristobalite overgrows the few relictic quartz grains, which suggest that its content could be below the XRD detection limit of 5%.

With the x100 objective, it was possible to get in some spots the pure signature of a glassy silicate with SiO_4 stretching components at ~790(weak), 920(shoulder), 995(shoulder), 1050 (strong) and 1220 cm^{-1} (shoulder) [20,21] (Fig. 2). Surprisingly, some characteristic peaks of lead arsenate apatite (a strong 820 cm^{-1} peak and a ~780 cm^{-1} shoulder, Fig. 2d) [23], see discussion below, were also recorded in the body, far away from the enamel. Were some blue pigments added to the paste to whiten it or did the enamel infiltrate the body along a crack? The nature of the green body (sand, frit and small amount of marl) may promote crack formation.

3.2. Transparent glaze

β-pseudowollastonite was observed with variable intensity in many spectra (Figs. 3–6), as expected for soft-paste (frit) porcelain [11–13]. The tiny peak at ~995 cm^{-1} can be due to traces of α − wollastonite and the one at ~1000 cm^{-1} can be the signature of a stressed zircon ($ZrSiO_4$; expected at 1005 cm^{-1}) [24]. Their low content prevents observing other peaks and hence a reliable assignment. Zircon is a common minor phase in sands and clays. Its exceptional chemical stability prevents reactions with other phases during the firing. Traces of α-quartz were observed (465 cm^{-1}) in some spectra, especially in yellow and blue enamels (Fig. 3b-left & a-right).

3.3. Enamels

Characteristic Raman spectra were obtained on blue, yellow, green, orange, violet(mauve) and "black" enamels, and on the transparent glaze at the surface or on the fracture (Figs. 3 and 4). Spectra recorded on the purple enamels didn't show well defined peaks due to the strong absorption of the laser light by Au° nanoparticles and thus the contribution of fluorescence emission superimpose to the Raman signal. The decrease of fluorescence under blue excitation (Fig. 5, the higher

Table 2
Phases identified by Raman microspectroscopy.

Phase	Formula	Location	Main peak (cm^{-1})	Intensity
wollastonite	α-$CaSiO_3$	glaze	995	very weak
pseudowollastonite	β-$CaSiO_3$	body	640,975	strong
		glaze	idem	strong
α-quartz	SiO_2	body	~465	almost not detected
		glaze		weak
		enamel	idem	weak
tridymite	SiO_2	body	~345	weak
α-cristobalite	SiO_2	body	230, 415	strong
β-cristobalite	SiO_2	body	830 (broad)	very weak
zircon	$ZrSiO_4$	glaze	1005	very weak
apatite	$Na_{0.4}K_{0.1}Ca_{0.5}Pb_4(AsO_4)_3$	body	~820	weak
		blue, green enamels	~820	strong
pyrochlore	$PbSn_xSb_{2-x}O_{7-\delta}$	yellow, green, orange	~138,512	strong
hematite	$Fe_{2-x}M_xO_3$	orange	~220,285,1315	weak
carbon	C	'black'	1360 – 1585	weak
lead-alkali glass	See text	body	~1050	strong
		glaze	idem	strong
Lead glass	See text	glaze	~985	strong

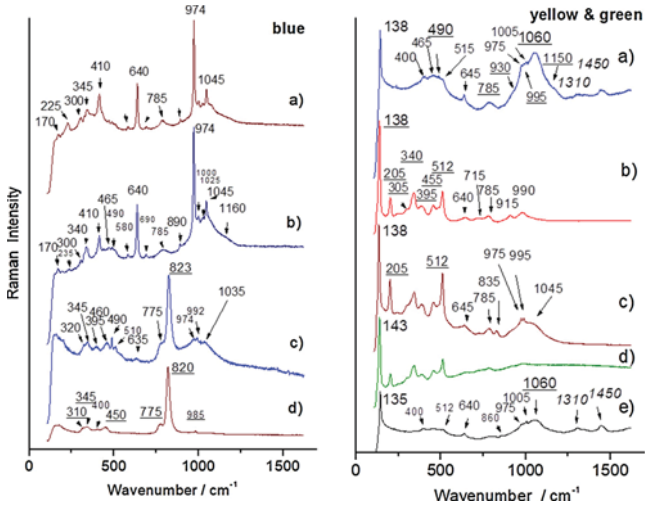

Fig. 3. Left, representative spectra recorded under green laser excitation on blue enamels (a and c, at the surface; b, on fracture section below the blue area, i.e. on the glaze, see Fig. 1a); (d), on fracture, blue grain. Right, representative spectra recorded on yellow (a,b,d) and green (c,e) enamels. (b, c and d = surface measurements; a and e = measurements on the fracture sections). (For interpretation of the references to color in this figure legend, the reader is referred to the web version of this article.)

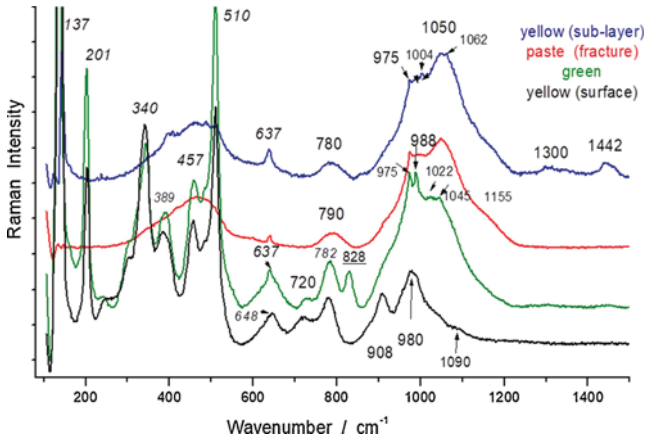

Fig. 4. Comparison of glassy silicate Raman spectra recorded under green laser excitation measured on the sections after a baseline subtraction (wavenumbers in italics correspond to pigments). (For interpretation of the references to color in this figure legend, the reader is referred to the web version of this article.)

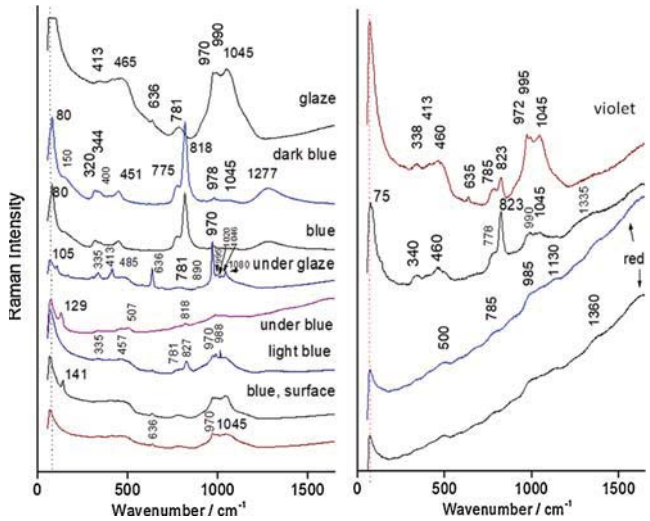

Fig. 5. Representative Raman spectra recorded under blue laser excitation at the surface for blue, violet and red/purple overglazes (dot line shows the limit of the experimental spectral window). (For interpretation of the references to color in this figure legend, the reader is referred to the web version of this article.)

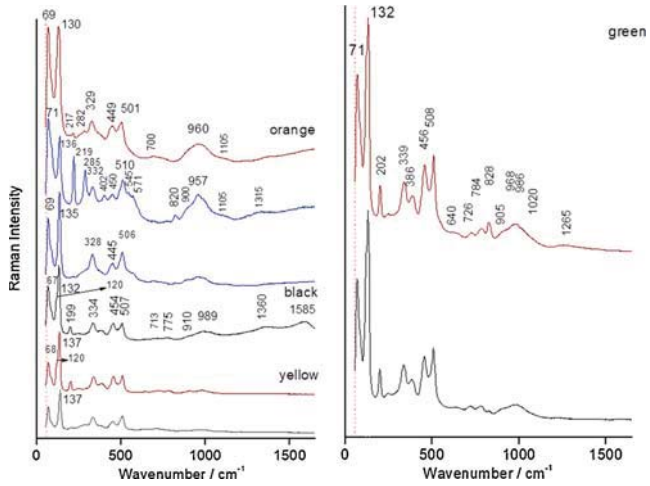

Fig. 6. Representative Raman spectra recorded under blue laser excitation at the surface of glaze and enamels (dot line shows the limit of the experimental spectral window). (For interpretation of the references to color in this figure legend, the reader is referred to the web version of this article.)

energy of the laser clean the sample surface from pollution and hence increases the quality of the signal) allows collecting some information: a strong diffusion is observed below 100 cm^{-1} because the contribution of the intense Lamb's modes of the metal nanoparticles [6,25]. The contribution of the glassy matrix is detected with bumps at ~500 (bending Si-O modes) and 985 to 1130 cm^{-1} (stretching Si-O modes) [20,21] The violet/mauve colour spectrum shows a signature intermediate between that of blue and of purple (Fig. 5), see below.

In the blue enamels a strong peak at ca. 820 to 823 cm^{-1} with a shoulder at ~775 cm^{-1} is present (Fig. 3c,d). In some spots of dark blue areas (Fig. 3d, left; Fig. 5) with x100 objective (i.e. analysed volume ~5 × 5x15 μm^3), a spectrum free of the contribution of the glassy silicate matrix exhibits peaks characteristics of $Na_{1-x}K_xPb_4(AsO_4)_3$ apatite [23] at 80, 320, 345, 450, 775, 822 and 985 cm^{-1}. Under blue laser excitation an additional feature is observed at 1277 cm^{-1}. This is consistent with a resonance Raman Effect. The huge intensity of As-O symmetric stretching mode arises from the high number of electrons involved in the bond (Z_{As} = 33).

The yellow, green and orange enamels show the characteristic signature of Naples Yellow pyrochlore ($Pb_2Sb_{2-x-y}Sn_xM_yO_{7-\delta}$solid solution) with its strong peak at ~138 cm^{-1} involving vibration of (heavy) Pb^{2+} ions [26–31]. The well defined and strong peak at 512 cm^{-1} observed in many spectra (Figs. 3 and 6) indicates that the solid solution is Sb-rich (Tin-rich composition exhibits a stronger 450 cm^{-1} peak [26–31]). Because the pyrochlore structure depends either from the composition and the firing conditions, it is difficult to deduct more precisely the composition from the Raman measurements. Spectra of the green enamel exhibit additional signature of the blue phase (~830 cm^{-1} peak), according to the preparation of the green colour by mixing the yellow pigment and a blue glass as commonly observed for 18th century artefacts [12] and documented by SEM-EDS for the analysed specimens [8]. The small wavenumber upshift may arise from compositional changes and/or tensile stresses imposed by the glassy matrix. The "black" line of the drawing limits the coloured areas. In fact, optical analyses show that these lines consist of a violet stripe over the green enamel [see in ref. 10, Fig. 10b, c]. According to the Raman measurements carbon is present and identified by its doublet at 1360 –

Table 3
Composition of white globules as measured [8] and calculated for a Pb-As-apatite with the formula $Na_{0.4}K_{0.1}Ca_{0.5}Pb_4(AsO_4)_3$, all in wt.%.

Na_2O	K_2O	CaO	PbO	As_2O_3	other	
2.6	0.9	2.9	67	17.1	9.5	measured
2.0	0.8	2.3	70	24	–	calculated

1585 cm^{-1} (Fig. 6-left). Carbon is very difficult to burn in condensed matter (carbon oxidation in covalent oxide requires temperatures higher than 1100 °C). It represents most likely a residue of incompletely burned gum arabic, with which the glass powders of the enamel colours were mixed, and not a specific pictorial pigment and commonly observed in enamelled porcelains [32]. It could be also a remnant of turpentine used by a restorer. Orange to red areas exhibit spectra with a small bump at 1315 cm^{-1} (Fig. 6, left) which can be consistent of some addition of hematite [11,12]. This is also consistent with the 219-285 cm^{-1} doublet (Fig. 6, left), characteristic of Al or Ti substituted hematite [33].

Broad bands at ~460 and 900 to 1100 cm^{-1} are characteristic of amorphous silicates [20,21]. Two types of glassy matrix are distinguished: (1) a lead-rich glass with stronger Si-O stretching component at 990 cm^{-1} (Fig. 3b-right, overglaze enamel) and (2) a mixed alkali-lead-based glass (the 'glaze') with Si-O stretching band exhibiting two strong peaks at ca. 990 and 1050 cm^{-1} (Fig. 3c-left). Actually the Si-O stretching pattern is variable due to local compositional changes.

Lead-(tin)-antimonate yellow pigment appears as pseudohexagonal thin crystals [8], as usual [26], with sizes ranging mainly from 0.5 to 5 µm. This is consistent with the recording of spectra almost free of other phases with a x100 objective as observed in Figs. 3 and 6. The well defined 512 cm^{-1} peak (Fig. 3 left) is consistent with a Sb-rich Naples Yellow $PbSn_xSb_{2-x}O_{7-\delta}$ pyrochlore, according to the measured elemental composition [8], with Sb_2O_3/SnO_2 mass ratio = 1.77 and 2.07 for yellow and green spots, respectively. Generally, the ca. 512 cm^{-1} peak appears stronger in green than in yellow enamels (Fig. 6). Furthermore, the wavenumber of Pb modes in yellow enamels is actually a doublet, with components at 120 and 137 cm^{-1} (Fig. 6). This could indicate two different pyrochlore phases. In orange enamels (core of the flowers, Fig. 1) the intensity of the ca. 70 cm^{-1} peak can be stronger than that of the ca. 130 cm^{-1} one. Similar features have been observed in PbO saturated enamels of Islamic pottery [34]. However, due to the platelet shapes of the pyrochlore crystals, and their inferior dimensions with respect to the lasers spot, the intensity variations created by different orientations (polarisation effect) will be negligible. The intensity changes can therefore be related to the presence of different phases and/or different compositions.

Fig. 4 compares spectra exhibiting a strong signature of glassy phases. For a better comparison the baseline has been subtracted according procedure described in ref [35]. The 980 cm^{-1} peak and the 908 cm^{-1} component found in the yellow enamel are typical of a lead-rich glass [21,32,34,36,37], matching the ~50 wt% of PbO as measured by SEM-EDS [8]. On the contrary the spectra exhibiting a strong ca. 1050-1060 cm^{-1} component recorded in the body (Fig. 2c) and in the colourless glaze layer between the body and the enamels (Fig. 3a, c &e, right; Figs. 5 and 4) is characteristic of a glass containing a significant level of alkali and earth-alkali [21]. This agrees well with the 20.7 wt.% Alk. & Earth-Alk of the Pb-free body glass and the 10.9 wt.% Alk. & Earth-Alk. and the 40.9 wt.% PbO of the glaze as measured by SEM-EDS [8]. Intermediate mixed lead-alkali/earth-alkali glass is identified with equal intensity of ca. 990 and 1050 cm^{-1} components (see e.g. Iznik and Kütahya glazes [7,38]). The variation observed in the Raman spectra indicates that the composition fluctuates slightly from place to place.

SEM micrographs show a crystallization of lead arsenate mainly in the form of globules with diameter ranging from ~3 to 5 µm [8]. The blue spectrum (Figs. 3d and 5) is very similar to that of $Na_{0.5}K_{0.5}Pb_4(AsO_4)_3$ apatite as reported by [23]. The intensity of the ~775 cm^{-1} peak is, however, lower, indicating a slightly different composition, such as the insertion of calcium in the solid solution. Apatite and lead-arsenates phases have been already identified by Synchrotron µXRD in pottery enamels, namely in majolica [39–42]. For the here studied blue enamel, the highest Ca content was measured in the globules [8], see Table 3.

An apatite composition of $Na_{0.4}K_{0.1}Ca_{0.5}Pb_4(AsO_4)_3$ would relatively well match the data. However, a formulation of a lacunar apatite has been preferred, i.e. $(Na_{0.4}K_{0.1}Ca_{0.5}Pb)_2\ Pb_3(AsO_4)_3V_2$, with V = vacancy, as Pb ions can occupy two sites, one forming the wall of empty hexagonal tunnels and one coordinated with 6 AsO_4-tetrahedra, Na^+ and K^+ ions being located in the latter [23]. Observed small peak shifts, from ~820 to 823 cm^{-1}, could indicate slightly different apatite compositions. The recorded spectrum is rather similar to that of the silicate homologue below 500 cm^{-1} [43,44], where the vibrational signature is dominated by that of the covalent vibrational unit XO_4, with a dominant contribution of moving oxygen atoms. Only the pure X—O stretching mode was observed at higher wavenumbers (850 to 868 cm^{-1} as a function of compositions). This confirms the sensitivity of XO_4 stretching mode to the substitution of M cations in $M_{10}(XO_4)_6V_2$ lacunar apatites.

Clear Raman signatures of arsenic apatite were already observed in many blue Pb-rich enamels and glasses: 16th Medici porcelain [45], 18th century Chinese Yixing stoneware and 18th century Chinese Qing Dynasty porcelain [32,46–48], European porcelain [13,49,50], and 19th/20th century lead-based glazes and glasses [51]. This indicates that during the synthesis of the blue enamel, saturation of the molten lead glass with arsenic arising from the use of As-rich cobalt ores or voluntary addition to whiten the blue hue, led to the coexistence of two liquids, followed by the crystallization of Pb-As-apatite on cooling [8]. In blue 17th and early 18th century decorated soft paste porcelain [32], i.e. in cobalt-containing lead-based blue enamels, spectra characterized by a broadening of the main peak and its shift up to 835 cm^{-1} has been observed. Orientational disorder of XO_4-based structures easily led to broadening of XO_4 stretching modes and this type of disorder may be promoted by matrix stress on small grains [52]. TEM analyses are needed in order to see if the broadening and shift is due to the formation of small disordered crystals and/or to formation of another phase.

4. Conclusion

Raman microspectrometry allows the identification in a non-invasive way of almost all the phases identified previously by XRD and SEM-EDS [8]. In the body, Raman scattering detects cristobalite very well, although this phase was not found by XRD, most probably due to its low amount. Contrarily to XRD, where quartz was evidenced, no significant quartz signature was found by Raman in the body. This is explained by the formation of cristobalite at the quartz grain surface covering the quartz signature. Both α− and β-wollastonites were detected, as well as traces of zircon. On the contrary, tridymite, a phase revealed by XRD, is hardly detected by the Raman technique. The lead-arsenate phase in the blue (and green) enamel is unambiguously identified as apatite. Different glassy phases are evidenced, namely mixed lead-alkali glass in the body and as colourless glaze and lead-reach glass in overglaze enamels. Variation of signature from place to place arises from the inter-reaction between enamels and glaze. Raman mapping on polished section could give more information.

References

[1] N. Wood, Chinese Glaze, Their Origins, Chemistry, and Recreation, University of Pennsylvania Press, Philadelphia, 1999.
[2] W.D. Kingery (Ed.), Ancient Technology to Modern Science, Ceramic and

Civilization, vol. I, The American Ceramic Society Press, Columbus, 1984.
[3] Ph. Colomban, V. Milande, On site analysis of the earliest known meissen porcelain and stoneware, J. Raman Spectrosc. 37 (5) (2006) 606–613.
[4] N.Q. Liem, Ph. Colomban, G. Sagon, H.X. Tinh, T.B. Hoanh, Microstructure, composition and processing of the 15th century Vietnamese porcelains and celadons, J. Cult. Herit. 4 (3) (2003) 187–197.
[5] M. Tite, T. Pradell, A. Shortland, Discovery, production and use of tin-based opacifiers in glasses, enamels and glazes from the late iron age onwards: a reassessment, Archaeometry 50 (1) (2008) 67–84.
[6] Ph. Colomban, C. Truong, A non-destructive Raman study of the glazing technique in lustre potteries and faiences (9th-14th centuries): silver ions, nanoclusters, microstructure and processing, J. Raman Spectrosc. 35 (3) (2004) 195–207.
[7] Ph. Colomban, V. Milande, L. Le Bihan, On-site Raman analysis of Iznik pottery glazes and pigments, J. Raman Spectrosc. 35 (7) (2004) 527–535.
[8] M. Maggetti, A. d'Albis, Phase and compositional analysis of a Sèvres soft paste porcelain plate from 1781, with a review of early porcelain techniques, Eur. J. Mineral. 29 (3) (2017) 347–367.
[9] V. Tadenevska, Ph. Colomban, B. Minceva-Sukarova, O. Grupce, Characterization of pottery from Republic of Macedonia, I: Raman analysis of Byzantine glazed pottery excavated from Prilep and Skopje (12th-14th century), J. Raman Spectrosc. 40 (9) (2009) 1240–1248.
[10] R. Trittschack, M. Maggetti, A. d'Albis, G. Kozlowski, Analyse d'une assiette peinte par Jean-Jacques Pierre le Jeune à Sèvres en 1781, Mitteilungsblatt Keramikfreunde der Schweiz 129 (2015) 50–62.
[11] Ph. Colomban, F. Treppoz, Identification and differentiation of ancient and modern European porcelains by Raman macro- and microspectroscopy, J. Raman Spectrosc. 32 (2) (2001) 93–102.
[12] Ph. Colomban, I. Robert, C. Roche, G. Sagon, V. Milande, Identification des porcelaines "tendres" du 18ème siècle par spectroscopie Raman: Saint-Cloud, Chantilly, Mennecy et Vincennes/Sèvres, Revue d'Archéométrie 28 (2004) 153–167.
[13] D. Mancini, C. Dupont-Logié, Ph. Colomban, On-site identification of Sceaux porcelain and faience using a portable Raman instrument, Ceram. Int. 42 (13) (2016) 14918–14927.
[14] P. Richet, B.O. Mysen, High-temperature dynamics and carnegieite ($NaAlSiO_4$) in cristobalite (SiO_2): a Raman spectroscopy study, Geophys. Res. 26 (15) (1999) 2283–2286.
[15] D.C. Palmer, R.J. Hemley, C.T. Prewitt, Raman spectroscopic study of High-pressure phase transitions in cristobalite, Phys. Chem. Minerals 21 (8) (1994) 481–488.
[16] D.C. Hezel, H. Palme, L. Nasdala, F.E. Brenker, Origin of SiO_2-rich components in ordinary chondrites, Geochim. Cosmochim. Acta 70 (6) (2006) 1548–1564.
[17] E. Bourova, P. Richet, Quartz and cristobalite: high-temperature cell parameters and volumes of fusion, Geophys. Res. 25 (13) (1998) 23333-2336.
[18] M. Ostrooumov, A Raman, infrared and XRD analysis of the instability in volcanic opals from Mexico, Spectrochim. Acta Part A 68 (2007) 1070–1076.
[19] W.D. Kingery, H.K. Bowen, D.R. Uhlmann, Introduction to Ceramics, Ch. 11, Microstructure of Ceramics, J. Wiley & Sons, New-York, 1975 p.538.
[20] Ph. Colomban, Polymerisation degree and Raman identification of ancient glasses used for jewellery, ceramics enamels and mosaics, J. Non-Cryst. Solids 323 (1-3) (2003) 180–187.
[21] P. Colomban, A. Tournié, L. Bellot-Gurlet, Raman identification of glassy silicates used in ceramic, glass and jewellry: a tentative differentiation guide, J. Raman Spectrosc. 37 (8) (2006) 841–852.
[22] G. Gouadec, Ph. Colomban, Raman spectroscopy of nanomaterials: how spectra relate to disorder, particle size and mechanical properties, Prog. Cryst. Growth Charact. Mater. 53 (1) (2007) 1–56.
[23] B. Manoun, M. Azdouz, M. Azrour, R. Essehli, S. Benmokhtar, L. El Ammari, A. Ezzahi, A. Ider, P. Lazor, Synthesis, Rietveld refinements and Raman spectroscopic studies of tricationic lacunar apatites $Na_{1-x}K_xPb_4(AsO_4)_3$ ($0 < x < 1$), J. Mol. Struct. 986 (1–3) (2011) 1–9.
[24] C. KarrJr (Ed.), Infrared and Raman Spectroscopy of Lunar and Terrestrial Minerals, Academic Press-Elsevier, New-York, 1975.
[25] G. Simon, L. Meziane, A. Courty, Ph. Colomban, I. Lisiecki, Low wavenumber Raman scattering of cobalt nanoparticles self-organized in 3D superlattices far from surface plasmon resonance, J. Raman Spectrosc. 47 (2) (2016) 248–251.
[26] M. Pereira, T. de Lacerda-Aroso, M.J.M. Gomes, A. Mata, L.C. Alves, Ph. Colomban, Ancient Portuguese ceramic Wall tiles (« Ajulejos »): characterization of the glaze and ceramic pigments, J. Nano Research 8 (2009) 79–88.
[27] C. Sandalinas, S. Ruiz-Moreno, A. Lopez-Gil, J. Miralles, Experimental confirmation by Raman spectroscopy of a Pb-Sn-Sb triple oxide yellow pigment in sixteenth-century Italian pottery, J. Raman Spectrosc. 37 (10) (2006) 1146–1153.
[28] F. Rosi, V. Manualli, C. Milliani, B.G. Brunetti, A. Sgamellotti, T. Grygar, D. Hradil, raman scattering features of lead pyroantimonate compounds. Part I: XRD and Raman characterization of $Pb_2Sb_2O_7$ doped with tin and zinc, J. Raman Spectrosc. 40 (1) (2009) 107–111.
[29] C. Pelosi, G. Agresti, U. Santamaria, E. Mattei, Artifical yellow pigments: production and characterization through spectroscopic methods of analysis, ePreservationScience 7 (2010) 108–115.
[30] Ph. Colomban, L. Arberet, B. Kirmizi, On-site analysis of 17th - 18th centuries Limoges enamels. Arsenic and the technological relationship between enamelled Limoges and Chinese wares, Ceram. Int. 43 (13) (2017) 10158–10165.
[31] M.C. Caggiani, C. Valloteau, Ph. Colomban, Inside the glassmaker technology: search of Raman criteria to discriminate between Emile Gallé and Philippe-Joseph Brocard enamels and pigment signatures, J. Raman Spectrosc. 45 (6) (2014) 456–464.
[32] Ph. Colomban, T.-A. Lu, V. Milande, Non-invasive on-site raman study of blue-decorated early soft-paste porcelain: the use of arsenic-rich (European) cobalt ores – comparison with *huafalang* Chinese porcelains, Ceram. Int. 44 (8) (2018) 9018–9028.
[33] F. Froment, A. Tournié, Ph. Colomban, Raman identification of natural red to yellow pigments: ochre and iron-containing ores, J. Raman Spectrosc. 39 (6) (2008) 560–568.
[34] Ph. Colomban, G. Sagon, A. Louhichi, H. Binous, N. Ayed, Identification par microscopie Raman des tessons et pigments de glaçures de céramiques de l'Ifriqiya (Dougga, XI-XVIII ièmes siècles), Rev. d'Archéomètrie 25 (2001) 101–112.
[35] Ph. Colomban, On-site Raman identification and dating of ancient glasses: a review of procedures and tools, J. Cult. Her. 9 (Suppl. S) (2008) e55–e60.
[36] G. Simsek, A.E. Geckinli, An assessment study of tiles from Topkapi Palace Museum with energy-dispersive X-ray and Raman spectrometers, J. Raman Spectrosc. 43 (7) (2012) 917–927.
[37] C. Viti, I. Borgia, B. Brunetti, A. Sgamellotti, M. Mellini, Microtexture and microchemistry of glaze and pigments in Italian renaissance pottery from Gubbio and Deruta, J. Cult. Her. 4 (3) (2003) 199–210.
[38] Ph. Colomban, R. de Laveaucoupet, V. Milande, On-site Raman analysis of Kütahya fritwares, J. Raman Spectrosc. 36 (9) (2005) 857–863.
[39] G. Papalardo, E. Costa, C. Marchetta, L. Pappalardo, F.P. Romano, A. Zucchiatti, P. Prati, P.A. Mando, A. Migliori, L. Palombo, M.G. Vaccari, No-destructive characterization of Della Robbia sculptures at the Bargello museum in Florence by the combined use of PIXE and XRF portable systems, J. Cult. Her. 5 (2) (2004) 183–188.
[40] T. Pradell, G. Molina, J. Molera, J. Pla, A. Labrador, The use of micro-XRD for the study of glaze color decorations, Appl. Phys. A 111 (1) (2013) 121–127.
[41] J. Pérez-Arantegui, M. Resano, E. Garcia-Ruiz, F. Vanhaecke, C. Roldan, J. Ferrero, J. Coll, Characterization of cobalt pigments found in traditional Valencian ceramics by means of laser ablation-inductively coupled plasma mass spectrometry and portable X-ray fluorescence spectrometry, Talanta 74 (5) (2008) 1271–1280.
[42] J. Pérez-Arantegui, B. Montull, M. Resano, J.M. Ortega, Materials and technological evolution of ancient cobalt-blue-decorated ceramics: pigments and work patterns in tin-glazed objects from Aragon (Spain) from the 15th to the 18th century AD, J. Eur. Ceram. Soc. 29 (12) (2009) 2499–2509.
[43] G. Lucazeau, N. Sergent, T. Pagnier, A. Shaula, V. Kharton, F.M.B. Marques, Raman spectra of apatites: $La_{10-x}\ Si_{6-y}(Al,Fe)_yO_{26\pm\delta}$, J. Raman Spectrosc. 38 (1) (2007) 21–33.
[44] A. Pons, E. Béchade, J. Jouin, M. Colas, P.-M. Geffroy, M. Smirnov, O. Masson, P. Thomas, I. Kagomiya, T. Asaka, K. Fukuda, A. Slodczyk, Ph. Colomban, Structural modifications lanthanum silicate oxyapatite exposed to high water pressure, J. Eur. Ceram. Soc. 37 (5) (2017) 2149–2158.
[45] Ph. Colomban, V. Milande, H. Lucas, On-site analysis of Medici porcelain, J. Raman Spectrosc. 35 (1) (2004) 68–72.
[46] J. Van Pevenage, D. Lauwers, D. Herremans, E. Verhaeven, B. Vekemans, W. De Clercq, L. Vincze, L. Moens, P. Vandenabeele, A combined spectroscopic study on Chinese porcelain containing Ruan-Cai colours, Anal. Methods 6 (2) (2014) 387–394.
[47] Ph. Colomban, Y. Zhang, B. Zhao, Non-invasive Raman analyses of *huafalang* and related porcelain wares. Searching for evidence for innovative pigment technologies, Ceram. Int. 43 (15) (2017) 12079–12088.
[48] Ph. Colomban, F. Ambrosi, A.-T. Ngo, T.-A. Lu, X.-L. Feng, S. Chen, C.-L. Choi, Comparative analysis of wucai Chinese porcelains using mobile and fixed Raman microspectrometers, Ceram. Int. 43 (16) (2017) 14244–14256.
[49] P. Ricciardi, Ph. Colomban, V. Milande, Non-destructive Raman characterization of Capodimonte and Buen Retiro porcelain, J. Raman Spectrosc. 39 (8) (2008) 1113–1119.
[50] H.G.M. Edwards, Ph. Colomban, B. Bowden, Raman spectroscopic analysis of an English soft-paste porcelain plaque-mounted table, J. Raman Spectrosc. 35 (8–9) (2004) 656–661.
[51] F. Koleini, I. Pikirayi, Ph. Colomban, Revisiting Baranda: a multi-analytical approach in the classification of sixteenth/seventeenth century glass beads from northern Zimbabwe, Antiquity 91 (357) (2017) 751–765.
[52] G. Collin, R. Comes, J.P. Boilot, Ph. Colomban, NASICON analog $Na_3Sc_2(PO_4)_3$; Thermal behaviour of the α, β and γ types structures, correlations and transitions, Solid State Ionics 28–30 (1988) 437–441.